Near-infrared resonance Raman excitation profile studies of single-walled carbon nanotube intertube interactions: A direct comparison of bundled and individually dispersed HiPco nanotubes

Michael J. O'Connell, Saujan Sivaram, and Stephen K. Doorn*
Chemistry Division, C-ACS, MS-J563, Los Alamos National Laboratory, Los Alamos, New Mexico 87545, USA
(Received 18 December 2003; revised manuscript received 1 March 2004; published 28 June 2004)

Complete Raman excitation profiles for single-walled carbon nanotube radial breathing modes were obtained for bundled HiPco carbon nanotube samples in the region from 700 to 985 nm excitation. Results are compared to similar profiles generated from individual carbon nanotubes dispersed in aqueous solution, allowing a direct determination of intertube interaction effects on electronic properties for 12 specific semiconducting nanotube chiralities. Redshifts in the excitation profiles (ranging from 54 to 157 meV) are observed on going from isolated individual to bundled nanotubes. Additionally, bundling is found to broaden the electronic transitions by an average factor of 2.4 compared to individualized nanotube bandwidths. These results compare well with recent theoretical predictions for bundling effects. An investigation of bundling effects on radial breathing mode frequencies for 17 different nanotube chiralities finds no evidence for significant perturbation of these frequencies resulting from intertube interactions. Our results demonstrate that previously reported radial breathing mode frequency shifts are apparent shifts only, resulting from redshifting of the resonant electronic transitions for bundled nanotubes. Bundle inhomogeneity, packing efficiency, orientational disorder, and symmetry reduction are indicated as important factors in determining the degree of intertube interaction.

DOI: 10.1103/PhysRevB.69.235415 PACS number(s): 61.46.+w, 73.22.−f, 78.30.−j

I. INTRODUCTION

Carbon nanotubes have significant potential for wide ranging materials applications based on their physical and electronic properties.[1] A thorough understanding of their electronic properties is critical to the development of their applications in nanophotonic, [2] sensor, [3] and molecular electronic devices.[4–6] Accurate estimates for electronic transition energies are required to correlate experimental characterization methods with identification of the nanotube (n,m) electronic type in a sample. Determination of (n,m) types present in a sample is an important part of evaluating nanotube production, processing, and purification methods, as well as for determining and understanding individual nanotube characteristics for device applications.

Raman spectroscopy has proven to be a powerful method for both gaining an understanding of the fundamental electronic structure of carbon nanotubes and for probing and assigning the compositions of samples. Through the resonance Raman effect,[7] Raman spectroscopy has been shown to be a sensitive probe of nanotube electronic structure. Strong resonance enhancement can be obtained from nanotubes through tuning of the excitation source wavelength to overlap the van Hove singularities present in the one-dimensional (1D) density of states[8] of different nanotube types. The electronic resonances are dependent on nanotube diameter and chirality,[8] resulting in only a subset of the total nanotube population being enhanced/detected for any given excitation wavelength.[9] Adding to the utility of Raman for nanotube characterization is the occurrence of the so-called radial breathing mode (RBM) in the low-frequency region ($100-400\ \mathrm{cm}^{-1}$). The RBM frequencies have an inverse dependence on nanotube diameter,[10] following the relationship shown in Eq. (1):

$$\omega_{\mathrm{RBM}} = C_1/d_t + C_2, \tag{1}$$

where C_1 is 223.5 nm cm^{-1} and C_2 is 12.5 cm^{-1} for HiPco produced[11] samples.[12] Thus, in addition to their sensitivity to nanotube electronic structure, Raman spectra may also be used to directly characterize the diameters present in a nanotube sample. Coupling of resonance Raman excitation data to RBM frequencies can lead to a nearly unambiguous assignment of (n,m) nanotube type to a given RBM feature.

A large number of studies have been performed that capitalize on these capabilities to probe electronic transitions and their coupling to different nanotube phonon modes.[9,13–23] A focus on RBM behavior has been used extensively for characterization of diameter distributions for monitoring production methods.[22–25] Raman has also been used extensively to monitor nanotube processing[26,27] and various separation methods.[28–31] A number of studies also have yielded results for assigning RBM features to specific (n,m) designations.[18,20,21,32–34]

These limited examples demonstrate the importance of Raman characterization of nanotubes, yet many fundamental Raman studies are complicated by the fact that the samples under study have consisted of bundled, rather than isolated nanotubes. The strong intertube van der Waals interactions that promote bundling[35,36] will also result in significant perturbation of the nanotube electronic structure. Bundling has the effect of both shifting and broadening the electronic transition energies.[37] The resultant increased overlap of the transitions results in a blurring or even wiping out of the individual van Hove features present in the nanotube electronic absorption spectrum of an ensemble sample. These transition energies can still be probed using resonance Raman enhancement profiles, but definitive assignment of the Raman spectral features to individual (n,m) indices becomes difficult, as the experimental features will likely be significantly per-

turbed from expected values based on theoretical predictions for isolated individual nanotubes. The drawbacks of intertube interaction and ensemble broadening of spectra have been overcome in some instances, for which Raman techniques on isolated individual tubes or small bundles have been developed.[17–21,32] Thorough enhancement profile studies using these methods, however, have been limited. A more complete understanding of intertube interaction effects on electronic structure and Raman spectra remains necessary.

A number of theoretical studies have been performed to address the effects of intertube interactions in bundles on the fundamental nanotube electronic structure.[38–41] Qualitatively, these studies agree that a shift in electronic transition energies is predicted, but accuracy in the predictions have suffered through use of a limited tight-binding theory for description of the nanotube 1D density of states. Recent results show that curvature and trigonal warping effects can be significant in determining nanotube electronic structure.[42–44] The importance of these effects have also been demonstrated in recent Raman studies as well.[32,45] Curvature effects were recently incorporated in an *ab initio* study of nanotube electronic structure that also included a study of intertube bundling effects.[42] The intertube interactions were found to decrease the band gap in bundled semiconducting nanotubes compared to their isolated counterparts. Furthermore, these interactions lead to a perpendicular dispersion to the familiar 1D density of states that leads to a predicted broadening of transitions occurring in bundled nanotubes. Only a limited set of experimental scanning tunneling microscope (STM)[46] and Raman measurements for one tube type,[47] however, were available for comparison.

Additional studies have extended the electronic perturbation work to examine the effects of bundling on the radial breathing mode vibrations as well.[48–53] These theoretical efforts have been motivated by experimental results that suggest the RBM increases in frequency upon bundling.[22,23,52–54] Pressure dependence studies have resulted in the conclusion that enhanced intertube interactions will result in increasing RBM frequency with pressure.[53] Further studies concluded, based on comparisons of Raman data to predicted transitions for a given nanotube-type coupled to expected RBM frequencies, that bundling results in a significant ($\sim$8%) upshift in observed frequency from what is expected for an isolated nanotube.[22,23,52,53,55] Unfortunately, these results rely heavily on the accuracy of theoretical predictions of transition energies that may be limited by use of tight-binding calculations that do not account for curvature effects. A direct comparison between bundled and isolated tube samples would more definitively address the question of whether or not RBM frequency changes are induced by intertube interactions.

One study addresses this question for a limited number of metallic nanotube types. Rao *et al.*[56] obtained Raman spectra for CS_2 suspended arc-produced nanotubes, with excitation at three different laser wavelengths. Results for individual solubilized nanotubes were compared to results for bundled solid samples. In contrast to previous work, these authors observed an apparent downshift in RBM frequency on going from isolated to bundled nanotubes. Rather than invoke a direct effect of bundling on RBM frequencies, Rao *et al.* explain their results in terms of the intertube interaction causing an upshift in transition energy for bundled tubes. This upshift in energy will bring a different set of nanotube types into resonance with the excitation frequency, resulting in an apparent change in RBM frequency due to a change in nanotube types that are now detected in the Raman spectrum.

Resolution of these conflicting analyses will require more extensive direct comparisons of Raman data between individualized and bundled nanotube samples. Moreover, it will be important to extend these studies to encompass semiconducting tubes to add to the experimental work done on metallic species.[56] More detailed enhancement profile comparisons will also provide important data for comparison and development of theoretical efforts at describing intertube interactions, and to solidify Raman-based chirality assignments, which have previously relied strongly on assumed knowledge of transition energies. The opportunity to carry out these studies has recently presented itself, with the advent of methods[37] for bulk suspension of isolated individual HiPco-produced nanotubes.[11] The study of HiPco tubes will also provide the opportunity to expand the Raman data base to nanotubes of somewhat smaller diameter than the arc- and laser oven-produced tubes that have formed the bulk of previous studies.

We present here results of complete near-infrared resonance Raman studies of HiPco produced nanotubes. Our experiments have allowed us to directly compare Raman enhancement profiles obtained in the region between 700 and 985 nm excitation for both bundled and solution-phase individualized nanotube samples. Our data provide a direct test of the theoretical results provided by Reich and co-workers,[42] as well as directly addresses the issue of intertube interaction effects on RBM frequencies. We are able to compare results for 12 different semiconducting nanotube chiralities. We find that, as predicted by Reich *et al.*,[42] the van Hove transition energies for semiconducting nanotubes are both shifted to lower energy and broadened in samples of bundled nanotubes. Moreover, we find significant agreement in the overall magnitude of the effect as well. Additionally, we find no significant change in RBM frequencies on going from isolated individuals to bundled nanotubes. Our results indicate, as in the work of Rao *et al.*,[56] that changes in resonant excitation conditions on going to a bundled sample can lead to an apparent RBM frequency shift that in reality does not change for a given tube type. Differences from previous work that appear in our data are discussed in terms of the variance in nanotube packing that occurs in a real inhomogeneous bundle, compared to the idealized packing structures addressed in theoretical descriptions.

II. EXPERIMENT

Preparation of the solution samples of isolated individual single-walled carbon nanotubes (SWNTs) was performed as published previously.[37] HiPco[11] carbon nanotubes (batches 89 and 104) from Rice University were suspended in aqueous sodium dodecyl sulfate (SDS) solution. Briefly, 1 wt.% surfactant was combined with 40 mg of nanotube material in 200 ml of water, high shear mixed for 1 h, and ultrasonicated

at 590 W for 10 min. The suspension was centrifuged for 4 h at 200 000 g using a swing bucket rotor. The resulting decant was isolated and used for subsequent Raman experiments. Our above use of the term "isolated" is not meant to imply that the individualized nanotubes are free of any environmental interactions with the surfactant/solvent, it is only meant to indicate that the individualized nanotubes in these samples are isolated from significant interaction with each other. The solution samples that were used for the Raman studies displayed strong band-gap emission, indicating that the nanotubes in these samples are isolated from significant intertube interactions.[12,37]

Preparation of the solid sample of bundled SWNTs was performed by suspending 10 mg of solid, unprocessed HiPco (batch 107) nanotubes from Rice University in 10 ml of isopropanol. The isopropanol suspension was added dropwise to a microscope slide and allowed to dry to form an opaque SWNT film.

Raman spectroscopy on the samples was performed with excitation from a Ti:Sapphire laser operating between 700 and 985 nm. A triple monochromator and charge-coupled device camera were used for spectral collection with 5 cm^{-1} resolution and 5 min integration times. Laser power at the sample was 15 mW. Raw spectra were background subtracted to remove the Rayleigh background or the overlapping broad emission features originating from the semiconducting SWNTs. Each Raman spectrum in the region from 125 to 400 cm^{-1} was fitted using a summation of Lorentzian peak shapes. Spectral intensities were then corrected for instrument response and ν^4 dependence. Spectra were also obtained for 4-acetamidophenol at all excitation wavelengths in an identical sampling geometry for use in frequency calibration and as a relative intensity reference for correcting nanotube spectra for instrument response.

III. RESULTS

In previous work we performed complete resonance Raman excitation profiles for the radial breathing modes of individually dispersed HiPco nanotubes in solution.[34] The excitation range of 700 to 985 nm yielded Raman spectra for vibrational modes coupled primarily to the second van Hove ($v2-c2$) transitions and a few to the first van Hove ($v1-c1$) transitions of semiconducting nanotubes. The results of that work allowed us to spectrally isolate and assign chirality for 22 separate semiconducting nanotube types. Past difficulties in making chirality assignments from ensemble measurements (due to broad overlapping transitions/vibrational modes) were overcome by obtaining Raman spectra at well-resolved energy spacings across the near-infrared region. This capability allowed us to in effect perform a two-dimensional spectral separation of individual chiralities. Thus, pairing a specific RBM frequency with an excitation profile maximum allowed us to assign (n,m) indices to individual spectral features with a high degree of confidence not available by making chirality assignments based only on measured RBM frequencies and the use of Eq. (1). A dramatic example of why pairing RBM frequency with transition energy is necessary for generating the most accurate assignments can be found by looking at the nanotube pair (13,3) and (9,8) (both with RBMs predicted at 203.6 cm^{-1}) or the pair (9,1) and (6,5) (both with RBMs predicted at 307.6 cm^{-1}). Without knowledge of the transition energies for these nanotube types, it is impossible to assign their chirality solely with the RBM data. However, we find that these chiralities can easily be distinguished from each other by applying the enhancement profile data. Their transition maxima are separated from each other by 40 nm [for the (13,3) and (9,8) types] and by 65 nm [for the (9,1) and (6,5) types].[12,34]

Recent semiempirical predictions (based on the functional dependencies appearing in descriptions of trigonal warping effects)[12,57] for the energy spacings of the first and second van Hove singularities for SDS solubilized HiPco nanotubes have provided excellent agreement with chirality assignments made on the basis of 2D fluorescence excitation/emission profile data. This approach has recently been found to provide accurate assignment for tube types found in laser vaporization-produced nanotubes as well.[58] A comparison of our experimentally determined RBM frequencies and excitation maxima with the fluorescence-based predictions for the nanotube chirality assignments we have made (based on our Raman excitation data for solution phase individualized nanotubes) is in excellent agreement. On average the agreement in RBM frequency is within $+/-1.2$ cm^{-1}, while excitation maxima agree within $+/-13$ meV,[34] providing a high degree of confidence in our assignments. This provides a strong basis for tracking identical chiralities observed in Raman data obtained on bundled nanotube samples.

It has been pointed out that curvature effects in small diameter nanotubes can cause significant deviation from the RBM frequency behavior described by Eq. (1),[59] thus potentially complicating chirality assignments. Effects are most pronounced for near-zigzag types and have been observed for a number of small diameter near-zigzag chiralities.[34] The smallest diameters present in our samples, however, are at the upper bound of where the curvature effects become significant, thus minimizing potential impact on the assignments. These effects, however, underscore the importance of combining RBM frequency data with transition maxima obtained from enhancement profiles to make accurate chirality assignments.

The results of the solution phase Raman experiments on isolated individuals are compared to those obtained for bundled samples in Fig. 1. The spectral features observed in this 3D plot can be conveniently grouped into four regions. As discussed previously,[34] the appearance of these groupings is a natural consequence of the chirality distribution of the electronic transitions, which cluster as deviations from a near-arm chair axis.[12] The observed behavior is also consistent with the oscillating response as a function of excitation energy of the first spectral moment observed by Kuzmany and co-workers[22] and Kukovecz *et al.*[23] for the RBMs. This oscillatory behavior arises from the dependence of the transition energy on the progression in nanotube diameters. The oscillation becomes apparent as an increase in diameter in observed $v2-c2$ transitions (Fig. 1, groups II, III, and IV) moves these energies out of our observation window, and moves smaller diameter tubes for the $v1-c1$ transitions (Fig. 1, group I) into the window.

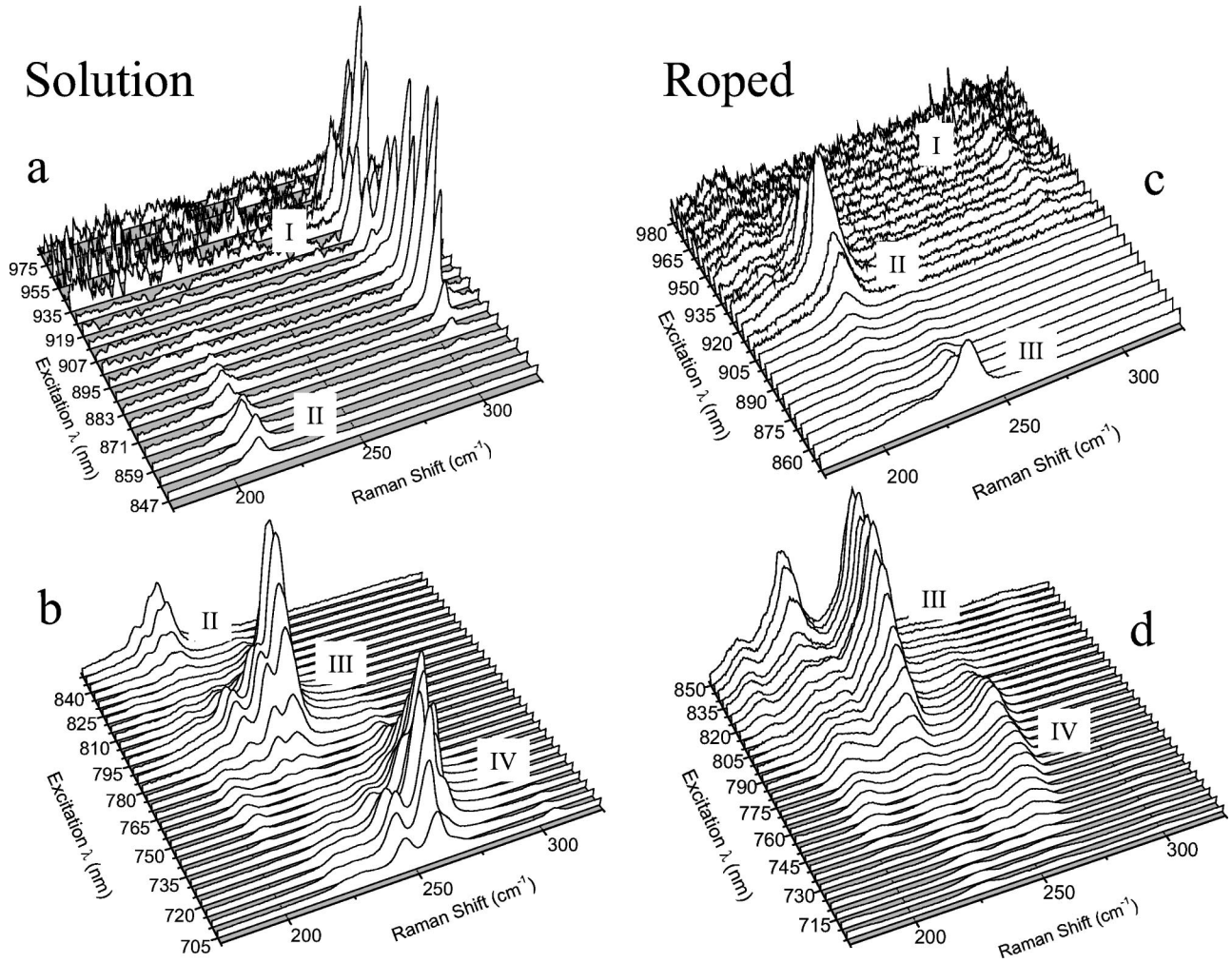

FIG. 1. Raman spectra of radial breathing modes for semiconducting nanotubes excited in the region of 700 to 985 nm for (a) and (b) individualized nanotubes in 1% SDS solution. (c),(d) Solid bundled nanotube sample.

On comparing the Raman data for the bundled nanotubes, we again observe the four groupings observed for the individualized samples. For the bundled tubes, however, all spectral features are shifted on the order of 30–50 nm to the red. There is also a blurring together of the regions labeled III and IV that is not observed for the individualized spectra. This blurring of transitions is an indication of band broadening occurring in the bundled sample. Although nominally we are accessing the same excitation region in the bundled sample, with primarily $v2-c2$ excitation with some $v1-c1$ resonances, the redshifting of the transitions changes the RBMs that are observable. This shift results in an incomplete overlap in data that is available for direct comparison between the two sample types. As a result, for the bundled sample, profile data for the (7,3), (6,5), and (8,3) nanotubes is not complete enough to obtain redshifted transition maxima. However, the tails of the excitation bands for the (6,5) and (8,3) chiralities are still observed, providing their RBM frequencies. Additionally, the redshifting allows access to $v2-c2$ transitions for bundled nanotubes that were to the blue of our observation window in the individualized samples. Nanotube types observable in this "new" window include the (8,0), (6,4), (8,3), and (7,5) chiralities. Sufficient data is present in the profile of the (8,3) nanotube in this region to provide the maximum in its $v2-c2$ excitation profile (Table I).

It is interesting to note that, with the exception of the (6,5), (13,3), and (11,7) nanotubes, we observe RBMs only for (n-m) mod 3=2 semiconductors (see Tables I and II). This is in contrast to a nearly equal distribution of (n-m) mod 3=1 and mod 3=2 types observed in the individualized sample. This is, however, consistent with the previous observation[34] that mod 3=1 types display significantly lower Raman intensity in the $v2-c2$ excitation region. This decreased intensity effect will be amplified for the bundled nanotubes due to broadening of their electronic transitions. The broadening will effectively yield lower Raman intensities due to a decreased electronic transition moment being spread over the width of the transition, thus making the mod 3=1 semiconductors for the most part unobservable in the bundled data. We also note that, for this reason, the only nanotube types not present in the current data set that were observed in the individualized samples[34] are of the mod 3 =1 type.

The data shown in Fig. 1 have been deconvoluted through Lorentzian fits to the individual Raman spectra and recom-

TABLE I. A comparison of Raman enhancement profile energy maxima and transition widths for individualized (solution) and roped nanotube samples.

(n,m)	Diameter nm	E (pred)[a] (cm^{-1})	E (soln)[b] (cm^{-1})	E (roped) (cm^{-1})	ΔE[c] cm^{-1}/(meV)	Width (soln) cm^{-1}/(meV)	Width (roped) cm^{-1}/(meV)
(9,1)	0.7573	10 964	11 050	10 492	558 (69)	369 (46)	622 (77)
(9,1)	0.7573	14 466	14 430	13 804	626 (78)		964 (120)
(8,3)	0.7819	15 029		14 286	743 (92)		
(10,2)	0.8841	13 574	13 717	12 883	834 (103)	446 (55)	883 (109)
(9,4)	0.9156	13 843	13 928	13 105	823 (102)	333 (41)	952 (118)
(8,6)	0.9658	13 928	13 967	13 534	433 (54)	432 (54)	763 (95)
(12,1)	0.9948	12 516	12 626	12 115	511 (63)	350 (43)	793 (98)
(10,5)	1.0503	12 695	12 739	12 209	530 (66)	370 (46)	936 (116)
(9,7)	1.1029	12 658	12 674	12 200	474 (59)	380 (47)	
(13,2)	1.120	11 661	11 669	10 830	839 (104)	112 (14)	363 (45)
(12,4)	1.145	11 693	11 696	10 874	822 (102)	278 (34)	757 (94)
(13,3)	1.170	13 095	13 263	12 708	555 (69)	466 (58)	724 (90)
(11,6)	1.1856	11 661	11 547	10 875	672 (83)		
(11,7)	1.2477	11 968	11 765	10 498	1267 (157)		713 (88)

[a]Predicted values obtained from Ref. 57.
[b]Experimental transition maxima for individualized solution samples obtained from Ref. 34.
[c]$\Delta E = E$(soln)-E(roped), except for (8,3) nanotube for which $\Delta E = E$(pred)-E(roped).

bined as enhancement profiles for individual RBMs shown in Figs. 2–4. High quality enhancement profiles were obtained with sufficient overlap between individualized and bundled samples to directly compare profiles for 12 separate nanotube chiralities, with one additional indirect comparison for the (8,3) $v2-c2$ transition. This direct comparison between the individualized and bundled Raman data is possible because we find a direct correspondence between the four spec-

TABLE II. A comparison of measured RBM frequencies for individualized (solution) and roped samples.

(n,m)	Diameter nm	v (pred.)[a] (cm^{-1})	v (soln)[b] (cm^{-1})	v (roped) (cm^{-1})	Δv[c] (cm^{-1})
(8,0)	0.6350	364.4		364	0
(6,4)	0.6921	335.4		333	−2
(6,5)	0.7573	307.6	307	307	0
(9,1)	0.7573	307.6	304	304	0
(8,3)	0.7819	298.3	296	296	0
(7,5)	0.8290	282.1		282	0
(10,2)	0.8841	265.3	264	266	2
(9,4)	0.9156	256.6	256	261	5
(8,6)	0.9658	243.9	244	244	0
(12,1)	0.9948	237.2	236	236	0
(10,5)	1.0503	225.3	225	227	2
(9,7)	1.1029	215.1	215	214	−1
(13,2)	1.120	212.1	211	213	2
(12,4)	1.145	207.7	206	209	3
(13,3)	1.170	203.6	205	203	−2
(11,6)	1.1856	201.0	200	201	1
(11,7)	1.2477	191.6	193	192	−1

[a]Predicted values obtained from Ref. 57.
[b]Experimental ν_{RBM} for individualized solution samples obtained from Ref. 34.
[c]$\Delta\nu = \nu$(roped)-ν(solen) except for (8,0), (6,4), and (7,5) nanotubes for which $\Delta\nu = \nu$(roped)-ν(pred).

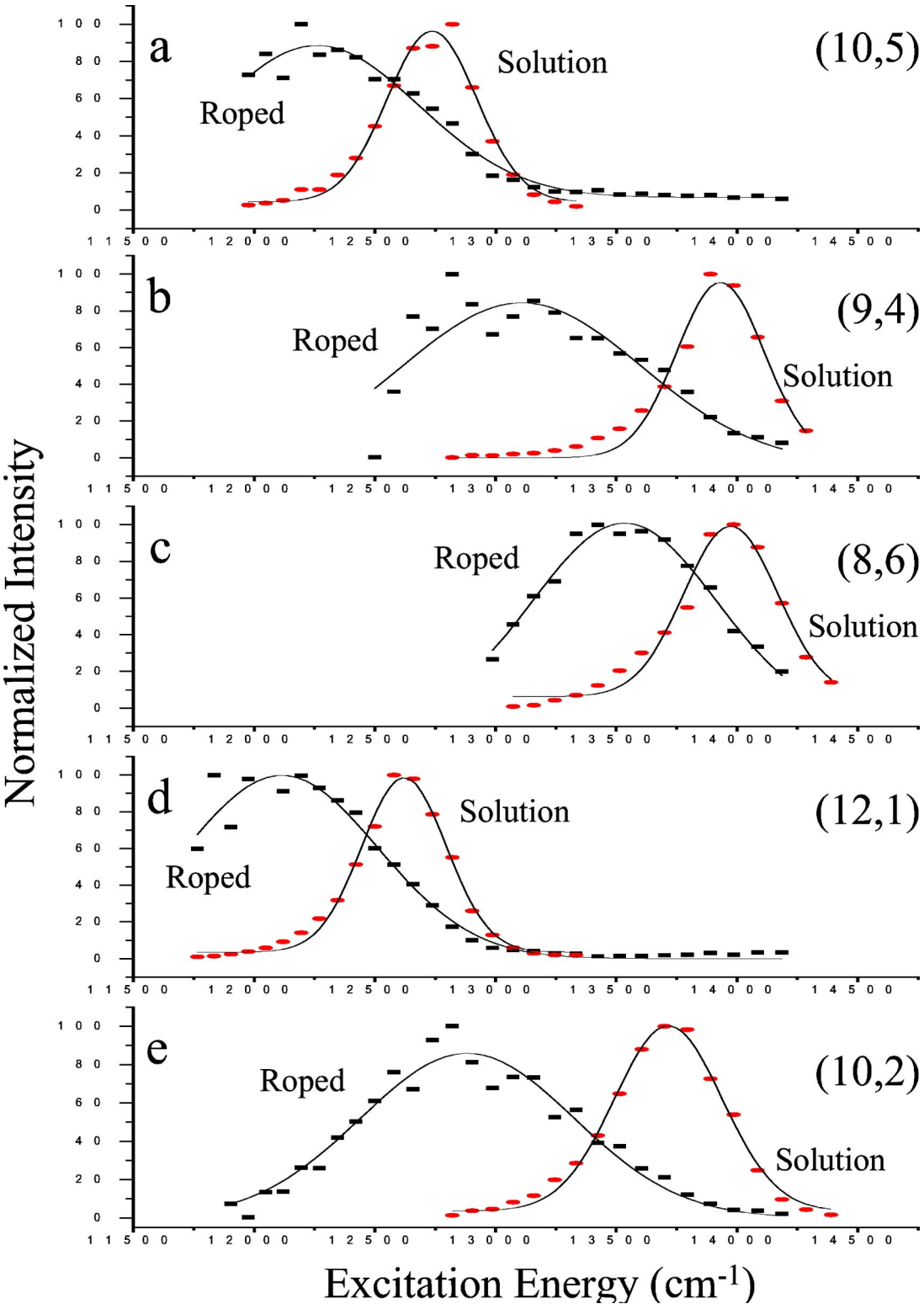

FIG. 2. (Color online) Comparison of Raman excitation profiles for individualized and bundled nanotubes for (a) (10,5), (b) (9,4), (c) (8,6), (d) (12,1), and (e) (10,2) chiralities (rectangles=roped data, ovals=individualized solution data).

tral groupings observed for each sample type in Fig. 1. The four groups found in the solution spectra are clearly preserved for the bundled sample (albeit with the bundled data broadened and shifted to the red). Moreover, the RBM frequencies within each spectral group track very closely for all groups when compared between the two sample types (see below and Table II).

Five of the enhancement profiles are compared for the $v2-c2$ excitation region between 700 and 850 nm in Fig. 2. We are able to sample the $v1-c1$ excitation only for the (9,1)

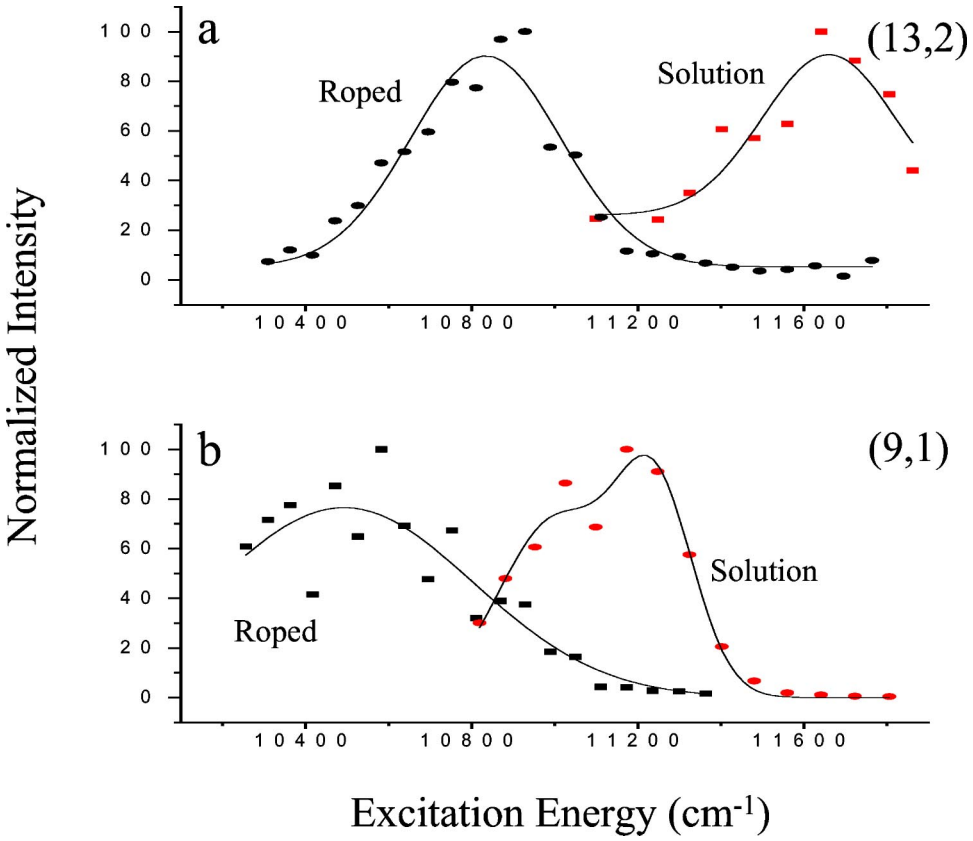

FIG. 3. (Color online) Comparison of low energy Raman excitation profiles for individualized and bundled nanotubes for (a) (13,2) and (b) (9,1) chiralities (rectangles = roped data, ovals = individualized solution data).

nanotube (see Fig. 3), while other chiralities shifted into the 850 to 985 nm region undergo $v2-c2$ excitation. Fortuitously, because of the shifting of transition energies that we observe, we are able to obtain partial enhancement profiles for both the $v1-c1$ and $v2-c2$ excitation regions of the (9,1) nanotube, providing a means for directly comparing differing effects of intertube interactions on both the $v2-c2$ and $v1-c1$ transitions for a single nanotube type (see Fig. 4). Simple Gaussian fits have been made to the profiles to obtain energy maxima and bandwidths for each observed electronic transition. Results for individualized and bundled samples are compared in Table I. For all chiralities except the (8,3) nanotube, the tabulated values for ΔE between individualized and bundled tubes are obtained directly from the experimental data.

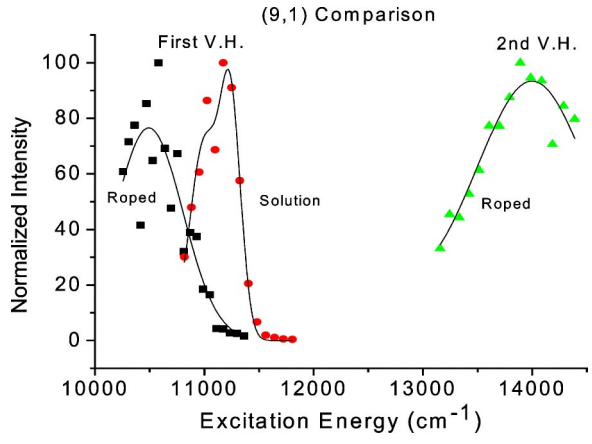

FIG. 4. (Color online) Comparison of Raman excitation profiles for individualized and bundled nanotubes for the (9,1) nanotube in the $v1-c1$ excitation range (first van Hove, squares = roped, circles = solution) and $v2-c2$ excitation range (second van Hove, triangles—roped only).

A pronounced redshift (ranging from 54 to 157 meV, with an average of 86 meV) for all transitions is clearly observed on going from individualized to bundled nanotubes for all tube chiralities. Transition widths are found to double and even triple (with an average factor of 2.4) for all chiralities on going from individualized to bundled nanotubes as well. One consequence of the band broadening for the (9,1) nanotube is that the structure observed due to phonon progressions[34] for the individualized sample is no longer observable once bundled [Figs. 3(b) and 4]. The combined effects of redshifting plus broadening of the electronic transitions creates significant changes in the observed RBM structure for bundled nanotubes as compared to individualized samples at any given excitation wavelength (see Fig. 5). The redshifting brings into resonance different nanotube chiralities in the bundled samples than are observed for individualized nanotubes. One additional effect the broadening has on the observed spectra is that chiralities that may not have been within the resonant window of a given excitation wavelength in the narrower band structure of the individualized nanotubes are now accessed due to the broadening of the transitions. As observed in Fig. 5, the resultant effect is to reduce the effective resolution of the Raman spectra in comparison to the sharper spectra observed for individualized samples. This is a result of more chiralities being at or near resonance at any given excitation wavelength for a bundled sample.

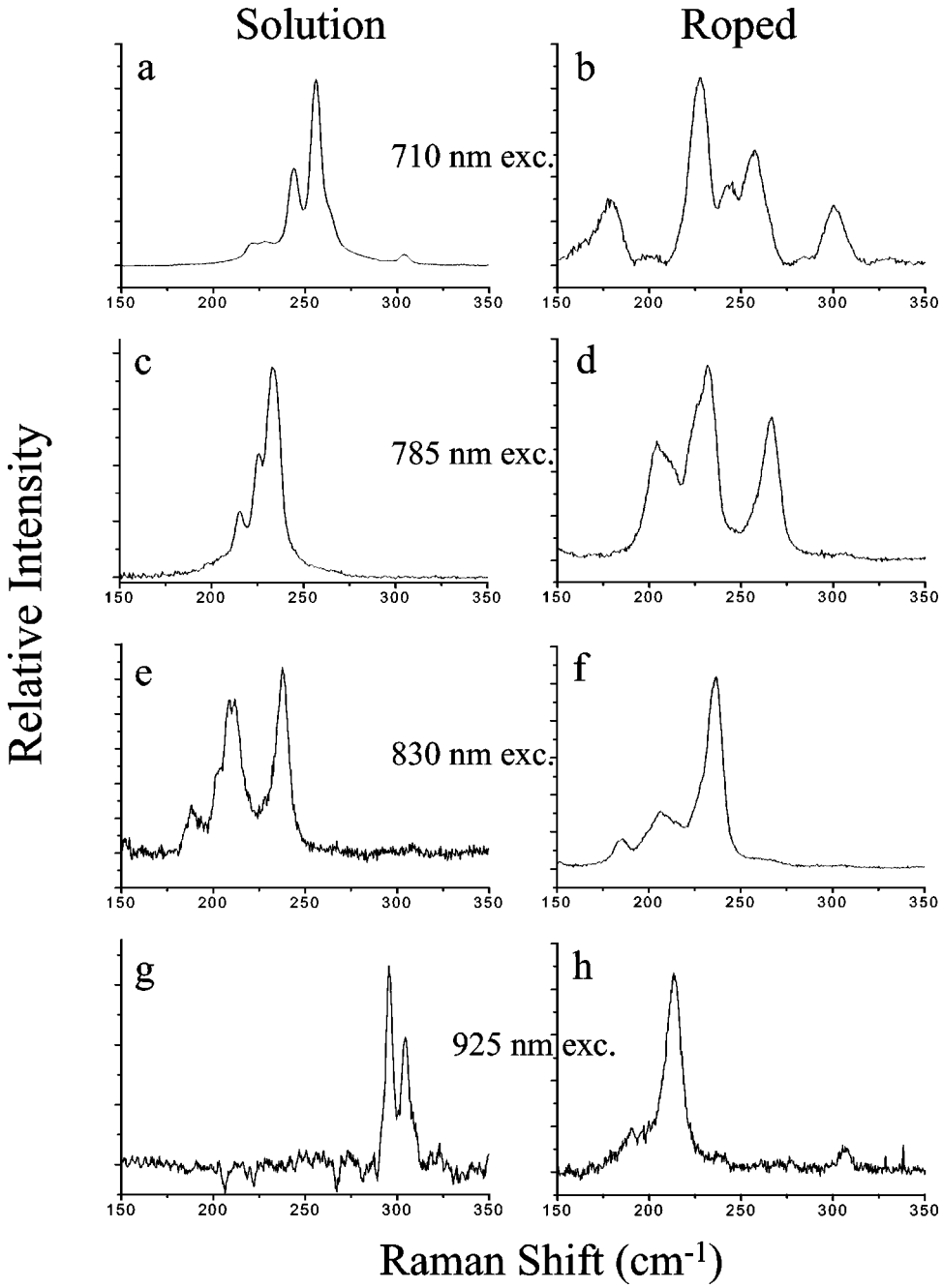

FIG. 5. Comparison of radial breathing mode spectra for individualized (solution) and roped (solid) nanotubes at four specific excitation wavelengths: 710 nm (a) solution, (b) roped; 785 nm (c) solution, (d) roped; 830 nm (e) solution, (f) roped; and 925 nm (g) solution, (h) roped.

In addition to being able to make a detailed comparison of intertube interaction effects on the nanotube electronic transitions, we have been able to compare RBM frequencies to determine whether or not the intertube interaction causes a change in vibrational frequency. As seen in Table II, we find no significant shift in vibrational frequency between individualized and bundled samples.

IV. DISCUSSION

A. Bundling effects on electronic transitions

As stated earlier, a number of theoretical studies on bundling effects have shown that transition energies in bundled nanotubes should be redshifted from those for their isolated counterparts.[48–53] Reich *et al.*[42] have incorporated curvature-induced hybridization effects into their studies of bundling, and have given detailed predictions for the magnitude of the transition energy shifts and bandwidth changes expected to occur upon bundling. For this reason, these results will be discussed more closely in relation to the data we present here. Trigonal warping has been shown to result in both positive and negative deviations in transition energies from what is expected from a strict tight-binding description, dependent on nanotube diameter, chirality, chiral angle, and transition regime ($v1-c1$ versus $v2-c2$).[12,44] For the specific systems evaluated by Reich *et al.* for bundling interactions, however, accounting for curvature in isolated nanotubes resulted in a decrease in energy separation between the valence and conduction band states relevant to the optical transitions ac-

cessed through resonance Raman excitation.[42] Intertube interactions in bundled systems were found to induce two additional effects: Changes in the electronic dispersion along k_z results in further decreases in the band gap for semiconducting nanotubes. Additionally, a dispersion perpendicular to k_z is found to occur, resulting in a broadening of the transition bandwidths.[42] Reich *et al.*,[42] as well as others,[38,40,41,56] also find that for armchair nanotubes intertube interactions lead to the opening of a pseudogap at the Fermi level.

The magnitude of these effects were found to be strongly dependent on nanotube type, with a range of armchair, zigzag, and chiral nanotubes being investigated. Bundling-induced shifts as large as 1 eV in certain armchair nanotube transitions are predicted, with effects being found to be smaller for zigzag and near-zigzag types. Effects on different individual transition energies within a given nanotube type were also found to vary widely, with higher energy transitions being less affected. The band-broadening effects of the perpendicular dispersion were found to be as large as 900 meV for armchair nanotubes, with the broadening being reduced for zigzag (no more than 400 meV) and smallest for chiral semiconducting nanotubes (less than 200 meV). In general, on closer inspection of the lowest van Hove transitions appearing in chiral semiconductors, of most relevance to the data we present, Reich *et al.* find a redshift on the order of 100 meV with an expectation of band broadening of not more than 200 meV.[42] This is in comparison to typical bandwidths of around 40 meV expected for isolated individuals in solution[12,33] and 20 meV obtained from excitation profiles on singly deposited nanotubes.[21]

The above calculated magnitudes for shifts in transition energies are in agreement with the work of Rao *et al.*,[56] who calculate an expected 200 meV shift in energies with an accompanying broadening as well. These researchers, however, find the shift to be a blueshift. The discrepancy may arise from differences in how the parameterized technique of Rao *et al.*[56] treats differences in single versus bundled nanotubes compared to the *ab initio* method of Reich *et al.*[42] The finding of Reich *et al.* that armchair nanotubes should display larger effects than those for zigzag nanotubes is in agreement with the results of Maarouf *et al.*[41] that coupling between near-armchair nanotubes is stronger than found for near-zigzag types.

The estimate of a 100 meV redshift in transition energies for chiral semiconducting nanotubes is in excellent agreement with our results. Our experimentally determined redshifts, ranging from 54 to 157 meV (see Table I) over a broad range of nanotube chiralities, compares within a factor of two of the predicted value from Reich *et al.*[42] We also observe the predicted broadening of the transitions on going to bundled samples as well. Our measured bandwidths on isolated nanotubes (44 meV on average, see Table I) agree with that expected for HiPco nanotubes in solution.[12,33] The isolated nanotube bandwidths increase by an average factor of 2.3, to range from 77 to 120 meV (see Table I). Although about a factor of 2 lower than the upper limit given by Reich *et al.* in their estimates,[42] the agreement still appears quite good. One observation of interest is that the magnitude of the observed redshifts and broadening is quite comparable over the range of nanotube types that we observe, from near-zigzag nanotubes such as the (9,1) and (12,1) to the near-armchair (8,6) and (9,7). This is in contrast to the large differences that might be expected between these types from Reich *et al.*[42] and Maarouf *et al.*[41] These predictions, particularly those of Reich *et al.*, are based on the assumption of direct interaction between identical nanotube types. The inhomogeneity expected for our samples, however, probably results in both a decrease in intertube interactions as well as the observation of more comparable effects of those interactions (see additional discussion below). Despite the narrow range observed for both redshifting and band broadening, there do exist significant differences in the effects observed for different chiralities. These differences may arise from interesting dependencies of the intertube interactions on nanotube type.

It is well known that nanotube chirality is a major determiner of a number of interesting behaviors. Thus, one might expect to observe unique chirality-based dependencies for intertube interactions as well. The effects of trigonal warping on nanotube transition energies effectively breaks the nanotube mod 3=1 and mod 3=2 types into two classes of separate behavior, depending on which van Hove transition is being excited.[12,44] Mod 3=1 types deviate to lower energy from a tight binding approximation, while mod 3=2 nanotubes deviate to higher energy for $v1-c1$ excitation. The sign of the deviation reverses on going to $v2-c2$ excitation. The magnitude of these deviations is determined by the nanotube chiral angle. This predicted behavior has been verified thru fluorescence measurements.[12] Similar dependencies are predicted[60] and observed[34] for Raman scattering cross sections as well, with behavior of mod 3=1 versus mod 3=2 types again reversing on going from $v1-c1$ to $v2-c2$ excitation. Other chirality dependent Raman processes have also been observed.[17,32] Additionally, for bundled nanotubes, there is the predicted variation in interaction dependence for armchair versus zigzag nanotubes, for which coupling/tunneling between nanotubes decreases as chirality changes from near armchair to near zigzag.[41,42]

As stated earlier, there is no clear delineation between near-armchair and near-zigzag behavior in our data. Additionally, we find no evidence for clear correlations between our observed redshifts and other chirality related dependences. Plots of ΔE between bundled and isolated samples as a function of chiral angle (α), $\cos(3\ \alpha)$, and $\cos(3\ \alpha)/d^2$ (the functional dependence for trigonal warping-induced deviations from tight-binding behavior)[12,44] show no correlation. This may be an indication that intertube interactions do not significantly perturb the C-C interaction energy (γ_0), as γ_0 acts as a scaling factor on the chiral angle dependence for trigonal warping effects.[12] This possibility has also been discussed previously by Rao *et al.*[56]

Our data, unfortunately, is not complete enough to evaluate whether or not there exist any significant differences in ΔE between mod 3=1 and mod 3=2 types. However, this issue may be addressed in part from the data obtained for the (9,1) nanotube. The (9,1) nanotube in the bundled sample provided profile data for both the $v1-c1$ and $v2-c2$ transitions (see Fig. 4). If there is a significant mod 3=1 versus mod 3=2 ΔE dependence, then that dependence might be expected to reverse itself between the two electronic transi-

tions accessed for the (9,1) nanotube. This would be in accord with the reversing of behavior on changing from $v1-c1$ to $v2-c2$ excitation that is observed for transition energies[12] and for Raman intensities[34] for the two separate mod 3 cases. As seen in Table I, though, the ΔE observed for both transitions is quite comparable, with ΔE's in the same direction (redshift) of 69 and 78 meV being found for the $v1-c1$ and $v2-c2$ transitions, respectively.

These results seem to indicate that there are no chirality specific effects for intertube interactions. This assertion must be qualified though with the understanding that chirality effects may be masked by the effects of decreased intertube interactions that might be expected for the inhomogeneous bundling that occurs in our roped sample. Raman,[9] STM,[46] and TEM[61,62] results all demonstrate that bundled samples will consist of a wide range of nanotube chiralities. The majority of theoretical bundling studies, however, have relied on formalisms that assume a perfect packing arrangement of identical tube types into a relatively high symmetry homogeneous bundle. That this assumption does not adequately represent the reality of the inhomogeneity found in real bundled samples has of course been recognized. Reich *et al.* have perturbed their calculations by rotating the nanotube orientations to break the D_{6h} symmetry of (6,6) bundles.[42] This orientationally disordered state results in a decreased effect on ΔE. Compositional disorder has also been recognized as reducing intertube interactions.[49,50] Maarouf *et al.* have focused on these disorder effects and again find that both orientational disorder and compositional inhomogeneity will reduce intertube interaction.[41]

In addition to compositional and orientational effects, loss of packing efficiency in inhomogeneous bundles may also reduce intertube interaction. Large diameter mismatches between adjacent nanotubes will lead to defects in a close packed bundle, as observed in bundle TEM images.[61,62] Short range order, however, may exist. Odom *et al.*[46] have shown through detailed STM measurements on nanotube bundles that nanotubes of similar chirality have a tendency to rope together. Likewise, nanotubes of similar diameter may be expected to aggregate together. However, a plot of ΔE as a function of diameter shows no correlation, indicating that any short range order effects do not dominate over the large-scale disorder sampled in our ensemble measurements.

B. Bundling effects on radial breathing mode frequencies

In addition to effects on nanotube electronic structure, bundling may also induce changes in the nanotube vibrational characteristics. We address here the question of whether or not RBM frequency changes result from nanotube bundling. Previous experimental results on laser ablation[22,52] and HiPco[23] produced nanotubes suggested that bundling can result in an upshift of the RBM frequency by as much as 8–10%. These conclusions were based on a comparison of experimental data to calculated spectra. Energy resonances for the calculated spectra were determined based on a tight-binding determination of density of states. Observed RBM frequencies were found to be, on average, 8.5% higher than predicted frequencies. The difference was attributed to bundling effects. Modeling of these effects by Henrard and co-workers[49,50] and Popov *et al.*[51] produced similar results, with predictions of frequency upshifts on the order of 10%.

Our experimental comparison of individualized and bundled nanotube samples, however, is in direct contradiction of the above conclusions. We find no significant evidence for a change in RBM frequency on going from individual nanotubes to bundles (see Table II). Our ability to directly track RBM behavior between solution and solid phase samples, rather than between experimental and predicted results, provides confidence in this conclusion. A remote possibility exists that any frequency upshifts that might occur on nanotube bundling could coincidentally result in an exact overlap of observed frequencies for the bundled nanotubes compared to the individualized sample. Such a coincidental overlap for all 17 RBMs, however, seems highly unlikely. Moreover, for the higher frequency RBMs (for example the 264 cm^{-1} mode in the individualized sample) a 5 to 10% upshift (to $\sim 280-290$ cm^{-1}) on bundling would result in the expectation of finding modes at higher frequencies that we do not observe. Our conclusion that nanotube bundling does not induce a significant change in RBM frequency is in agreement with the results of Rao *et al.*,[56] who also find no evidence for a bundling-induced change in RBM frequency.

There also exist a number of independent results in the literature that indicate that bundling and other environmental factors, such as solubilization environment, do not affect RBM frequencies. Raman data presented for capillary electrophoresis separations of nanotube bundles from individuals show that as bundle size steadily decreases to the single nanotube limit, RBM frequencies remain the same.[29] Additionally, RBM frequencies do not change when monitored during the ultrasonication debundling process used to create SDS solubilized nanotubes.[27] Finally, Raman data published for nanotubes wrapped in a variety of different surfactant and polymer systems (which result in significant changes in nanotube local environment, as evidenced by shifts in their emission spectra) show that RBM frequencies remain the same, independent of nanotube local environment.[63]

Our conclusions may be reconciled with the modeling results of Henrard and co-workers,[49,50] and Popov *et al.*[51] by again invoking sample inhomogeneity. Henrard *et al.* model intertube interactions using a Lennard-Jones potential between continuous cylindrical surfaces. Given the inhomogeneity of bundled nanotube samples, this model likely overestimates the interaction energies. Accounting for orientational and compositional disorder in bundles would likely improve the model. The Lennard-Jones potential will be sensitive to both the diameters and chiralities present in a bundle. As discussed in the section on bundling effects on transition energies, nanotube diameter mismatches will likely reduce packing efficiencies and intertube interactions. Additionally, intertube van der Waals forces will vary greatly with the ability of nanotube hexagonal geometries to be in perfect registry. As demonstrated by Odom *et al.*,[46] this high symmetry arrangement may occur within local domains, but within a large scale ensemble these domains are not likely to dominate. Lack of registry should reduce intertube interac-

tions. Thus, intertube interactions in an inhomogeneous bundle will be smaller than predicted using a continuous cylindrical approximation for nanotube interaction. The reduced interactions probably result in forces too small to induce a RBM frequency change. We do not claim that these frequency shifts cannot occur as a result of intertube interactions, it just may require more extreme conditions to generate the required interaction. In fact, such frequency upshifts are observed for nanotubes subjected to pressures on the order of GPa.[54] At ambient temperatures and pressures, however, interactions are too small to induce the frequency upshift.

The question remains of how can the experimental results of Kuzmany and co-workers,[22] Kukovecz *et al.*,[23] and Milnera *et al.*[52] be reconciled with our conclusion that RBM frequencies are not upshifted in nanotube bundles. In the work of Rao *et al.*[56] this apparent discrepancy in experimental results is explained in terms of changes in resonance excitation conditions on going from an individualized to bundled sample. These researchers correctly recognized that bundling will cause a shift in the electronic transition energies, resulting in a new set of nanotube chiralities that will be resonant with a fixed excitation wavelength. Thus, for any given excitation wavelength, one should expect a different set of RBMs to be present in spectra for individualized nanotubes as compared to a bundled sample (as we observe in Fig. 5). The difference in observed modes can easily be interpreted as an apparent change in RBM frequency if accurate knowledge of transition energies and bundling induced intertube perturbations are not accounted for. These results highlight the importance of arriving at correct predictions for energy levels in isolated nanotubes and for how bundling perturbs these levels. As noted by Reich *et al.*,[42] the errors introduced by using a tight-binding approach without compensation for curvature, hybridization, and trigonal warping effects, makes accurate assignment of chiralities based on resonance measurements difficult. This difficulty emphasizes the importance of being able to evaluate bundling effects through a direct comparison of experimental data obtained for both bundled and individualized nanotubes. Such a direct comparison will minimize errors in interpretation introduced by inaccurate chirality assignments based on transition energy predictions.

The detailed nature of our data further demonstrates how the red shift in transition energies that occurs on bundling can lead to an apparent change in RBM frequency (see Figs. 1 and 5). Figure 1 demonstrates, as was also observed by Kuzmany and co-workers,[22] Kukovecz *et al.*,[23] and Milnera *et al.*[52] that as excitation progresses from high to low energy we observe periodic minima in the RBM profiles. When these minima are passed, a general shifting to lower frequency of the RBMs is observed. This oscillatory behavior is a consequence of the periodicity observed in the van Hove transitions that result from the change in chiral angle dependence of the transition energies on moving from near-armchair to near-zigzag structures within a given group of nanotubes.[12] It is exactly this oscillatory behavior, combined with the smooth progression to lower transition energies as nanotube diameter increases, that gives rise to an apparent RBM frequency shift.

Figure 5 shows that the differing resonance conditions between individualized and bundled nanotubes can result in dramatically different RBM spectra observed for identical excitation wavelengths. It is easy to see how inaccurate chirality assignments can be given to individual RBM features when these are made based solely on the bundled nanotube data. A closer inspection of Fig. 1 leads to a more complete understanding of how the redshift in transition energies leads to an apparent upshift in RBM frequency. If one observes behavior around the 785 nm excitation region, for example, as bundling occurs the transition energies for group III are moved out of resonance and into the vicinity of transitions found for group II as isolated individuals. Similarly, the group IV transition energy region moves into resonance with the 785 nm excitation. As a result, one would expect the frequencies for group III (centered around 225 cm^{-1}) to undergo an apparent upshift to the group IV frequencies (centered around 260 cm^{-1}). The same behavior will occur at lower excitation energies, with the group II RBM frequencies (centered around 200 cm^{-1}) undergoing an apparent upshift to those of the group III frequencies. Although this analysis will of course be complicated by the transition broadening that occurs upon bundling, which results in broader, more complex RBM spectra, it is qualitatively correct in demonstrating the origin of the apparent RBM frequency upshift. It is interesting to note that, if one goes to low enough excitation energy, the apparent trend toward upshifting RBM frequencies is reversed as the smaller diameter semiconductor nanotubes are accessed through the $v1-c1$ excitation. In this case [for an excitation wavelength of 925 nm, see Fig. 5(d)] we observe a large apparent decrease in frequency from the 296 and 304 cm^{-1} modes observed for the (8,3) and (9,1) nanotubes of the solution sample on going to resonance with the 213 cm^{-1} RBM of the (13,2) nanotube in the bundled sample.

Conversely, a comparison of Raman spectra for individualized nanotubes to spectra for bundled nanotubes obtained at excitation wavelengths shifted to the red by the same magnitude as we observe for redshifting of the transitions (around 50–100 meV) may yield nearly identical spectra. This expectation is borne out in Fig. 6. Spectra of individualized nanotubes taken at three separate excitation wavelengths (780, 825, and 850 nm) compare well with spectra obtained for bundles at wavelengths shifted to the red by 68, 61, and 89 meV, respectively. Although this is a simplified analysis and complicated, again, by broadening effects, the comparison provides another illustration of how a redshift in transition energies can result in the apparent upshifts in RBM frequency.

To summarize, no evidence for bundling-induced RBM frequency upshifts is found after comparing Raman spectra for individualized and bundled nanotube samples. Our conclusions are similar to those found by Rao, *et al.*[56] Apparent frequency shifts observed by others are most likely the result of the redshifting of electronic transitions that we find for bundled nanotubes. Lack of a significant frequency upshift may be a further indication that bundling does not induce a change in γ_0.[52,56]

It should be noted that these conclusions (and the results of the previous section as well) are not ultimately dependent

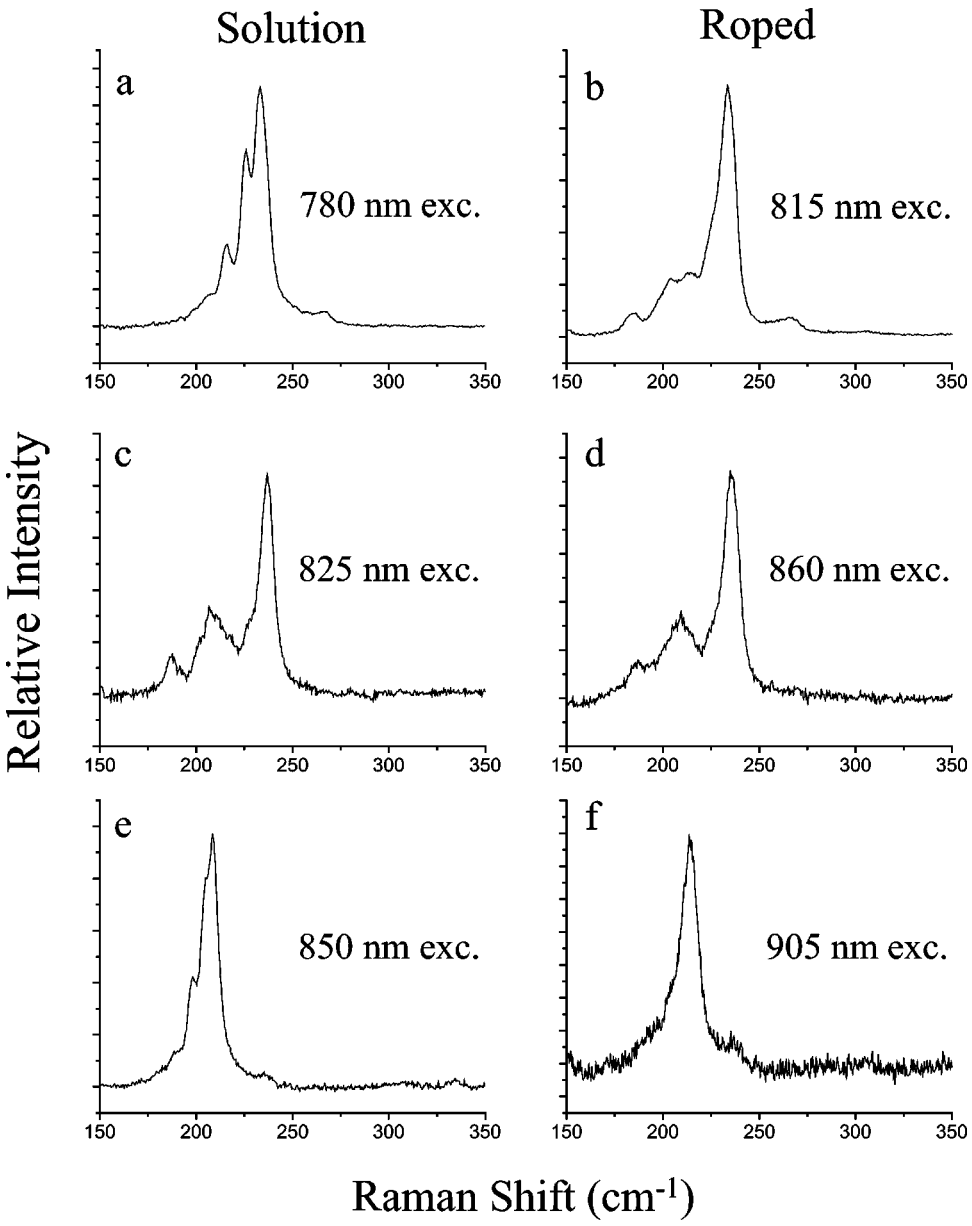

FIG. 6. Individual radial breathing mode spectra for individualized (solution) nanotubes at three excitation wavelengths compared to spectra for bundled nanotubes with excitation redshifted: (a) 780 nm (solution) versus 815 nm (roped), $\Delta E = 68$ meV, (b) 825 nm (solution) versus 860 nm (roped) $\Delta E = 61$ meV, and (c) 850 nm (solution) versus 905 nm (roped) $\Delta E = 89$ meV.

on accuracy of our chirality assignments. Although these assignments agree well with previous work[12,57,58] and are believed to be correct, ultimately our results are only dependent on the ability to directly track RBM behavior between the individualized and bundled samples through the detailed enhancement profiles and 3D Raman data of Fig. 1. This ability is independent of what chirality is ultimately assigned to the observed RBMs.

C. Practical considerations for sample characterization via Raman spectroscopy

Raman spectroscopy will continue to be an important characterization method for carbon nanotube applications. It is clear from Figs. 1 and 5 that a complete evaluation of a sample cannot be obtained with spectra collected from one excitation wavelength. Additionally, the differences presented by spectra obtained from bundled versus individualized samples adds complexity to the analysis. The data presented here should prove valuable in this regard. As one specific example, a focus on excitation behavior at 785 nm is useful. This wavelength is experiencing widespread use for Raman characterization of nanotube processing and separations,[26,29,64] due to its availability as a common diode laser excitation source with Raman instrumentation being designed around its use. On comparing the bundled and individualized spectra obtained at 785 nm excitation [Figs. 5(c) and 5(d)], the most noticeable difference is the strong presence of the (10,2) RBM at 266 cm^{-1} in the bundled sample, absent in the individualized nanotubes. This so-called "roping peak" can be used as a strong indicator of the extent of bundling occurring in a sample.[26,29] Results obtained from monitoring of capillary electrophoresis separations of nanotube bundles from individuals[29] and of the bundle sonication/solubilization process[26] demonstrate that, as bundle size decreases, a steady loss in the intensity of the 266 cm^{-1} (10,2)

RBM occurs relative to the (12,1) RBM at 236 cm^{-1}. Thus, a measurement of this intensity ratio could be useful in qualitatively estimating bundle size. The ability to quantify bundle size using this method would require more extensive analysis of samples of known bundle size coupled to modeling of expected RBM spectra as a function of relative levels of bundles versus individualized nanotubes.

It is interesting to note that the (12,1) RBM at 236 cm^{-1} appears strongly enhanced in both the individualized and bundled samples, while the roping peak is only present in the bundled form. This behavior results from the very different resonant excitation conditions experienced by the two different chiralities. As seen in Figs. 2(d) and 2(e), 785 nm (12 739 cm^{-1}) excitation is near the peak of the enhancement profile for the individualized (12,1) nanotubes. In the bundled sample, due to band broadening, this excitation still accesses significant resonant intensity in the tail of the (12,1) profile. The (10,2) nanotube, however, is only strongly resonant for the bundled sample, with 785 nm excitation missing the profile entirely for the isolated (10,2) nanotubes, due to the relative narrowness of the transition in the solution sample.

Because of the narrowness of the chirality distribution accessed with 785 nm excitation, this wavelength has limited utility as a monitor for changes in sample chirality. It can, however, serve as a valuable tool for evaluating the extent of aggregation occurring in a sample. It is important to be aware that these aggregation effects are present with 785 nm excitation, as well as for other commonly used wavelengths (such as 514, 532, and 633 nm). The extent of sample aggregation must be known in order to avoid assigning relative intensity changes between different chirality RBMs to a change in population, when it is possible that such intensity shifts may result from a shift in resonance enhancement conditions instead. To obtain full coverage of the range of chiralities present in a sample, it is not necessary to produce the detailed enhancement profiles presented here. As can be seen in Fig. 1, a judicious choice of 3–4 excitation wavelengths (735, 785, 850, and 920 nm, for example) can provide coverage for both individualized and bundled samples over a broad range of chiralities and diameters. Additionally, visible excitation such as at 514 and 633 nm can simultaneously access both metallic and semiconducting resonances, providing a means to evaluate relative levels of these important classes of nanotubes.[27,30,31,33]

V. CONCLUSION

We have presented data representing the first complete near-IR resonance Raman enhancement profiles for both individualized and bundled HiPco nanotubes. These have allowed us to demonstrate the redshifting and band broadening of the electronic transitions that have been predicted to occur upon nanotube bundling. Our results agree both qualitatively and semi-quantitatively with the expected magnitude of the electronic effects of bundling and provide further evidence for the importance of curvature-induced hybridization and trigonal warping effects on the nanotube density of states and electronic band structure.

Comparison of radial breathing mode frequencies for individualized and bundled nanotubes shows no significant change occurring in their frequencies as a result of bundling. Our analysis of changes in the excitation energy dependence between individualized and bundled nanotubes suggests that previously reported apparent frequency shifts are due to bundling-induced redshifts of the electronic transitions. Changes in nanotube RBMs enhanced in the new resonance conditions for bundled nanotubes can result in an apparent shift in RBM frequencies compared to their individualized counterparts. These results imply that current theoretical treatments of predicted vibrational effects overestimate the magnitude of intertube interactions.

Many previous studies have pointed out the potential importance of intertube interactions. Our results show this interaction to be most strongly manifested in effects on electronic properties. The lack of large differences observed for ΔE between different chiralities and different excitation regions, as well as the lack of a bundling-induced RBM frequency shift, suggests that orientational and compositional disorder in real nanotube samples are important factors in determining intertube interaction effects on both electronic and vibrational structure. Addressing inhomogeneity and other disorder effects on bundle properties will be an important area for future theoretical efforts. A more detailed understanding of interactions between different chiralities and the effects of imperfect packing, lack of registry, and lowered symmetry should lead to better modeling of true bundle behavior. These are important issues relating to both transport properties[41] and potential nanoelectronics and materials applications.

ACKNOWLEDGMENTS

This work was supported by the Los Alamos National Laboratory LDRD program. Raman spectroscopy was performed at the LANL Integrated Spectroscopy Lab. We wish to thank the Richard Smalley group at Rice University for supplying the carbon nanotube samples used in these studies.

*The author to whom all correspondence should be addressed; Electronic mail: skdoorn@lanl.gov

[1] B. I. Yakobson and R. E. Smalley, Am. Sci. **85**, 324 (1997).
[2] J. A. Misewich, R. Martel, Ph. Avouris, J. C. Tsang, S. Heinze, and J. Tersoff, Science **300**, 783 (2003).
[3] J. Kong, N. R. Franklin, C. Zhou, M. G. Chapline, S. Peng, K. Cho, and H. Dai, Science **287**, 622 (2000).
[4] R. Martel, T. Schmidt, H. R. Shea, T. Hertel, and P. Avouris, Appl. Phys. Lett. **73**, 2447 (1998).
[5] C. Niu, E. Sichel, R. Hoch, D. Moy, and H. Tennet, Appl. Phys.

Lett. **70**, 1490 (1997).
[6] A. Bachtold, P. Hadley, T. Nakanishi, and C. Dekker, Science **294**, 1317 (2001).
[7] R. M. Martin and L. M. Falicov, in *Light Scattering in Solids I*, edited by M. Cardona Chap. 3 (Springer, Berlin, 1983).
[8] R. Saito, G. Dresselhaus, and M. S. Dresselhaus, *Physical Properties of Carbon Nanotubes* (Imperial College Press, London, 1998).
[9] A. M. Rao, E. Richter, S. Bandow, B. Chase, P. C. Eklund, K. A. Williams, S. Fang, K. R. Subbaswamy, M. Menon, A. Thess, R. E. Smalley, G. Dresselhaus, and M. S. Dresselhaus, Science **275**, 187 (1997).
[10] M. S. Dresselhaus and P. C. Eklund, Adv. Phys. **49**, 705 (2000).
[11] M. J. Bronikowski, P. A. Willis, D. T. Colbert, K. A. Smith, and R. E. Smalley, J. Vac. Sci. Technol. A **19**, 1800 (2001).
[12] S. M. Bachilo, M. S. Strano, C. Kittrell, R. H. Hauge, R. E. Smalley, and R. B. Weisman, Science **298**, 2361 (2002).
[13] M. Canonico, G. B. Adams, C. Poweleit, J. Menendez, J. B. Page, G. Harris, H. P. van der Meulen, J. M. Calleja, and J. Rubio, Phys. Rev. B **65**, 201402 (2002).
[14] L. Alvarez, A. Righi, T. Guillard, S. Rols, E. Anglaret, D. Laplaze, and J. L. Sauvajol, Chem. Phys. Lett. **316**, 186 (2000).
[15] L. Alvarez, A. Righi, S. Rols, E. Anglaret, and J. L. Sauvajol, Chem. Phys. Lett. **320**, 441 (2000).
[16] M. A. Pimenta, A. Marucci, S. D. M. Brown, M. J. Matthews, A. M. Rao, P. C. Eklund, R. E. Smalley, G. Dresselhaus, and M. S. Dresselhaus, J. Mater. Res. **13**, 2396 (1998).
[17] R. Saito, A. Jorio, J. H. Hafner, C. M. Lieber, M. Hunter, T. McClure, G. Dresselhaus, and M. S. Dresselhaus, Phys. Rev. B **64**, 085312 (2001).
[18] A. Jorio, C. Fantini, M. S. S. Dantas, M. A. Pimenta, A. G. Souza, G. G. Samsonidze, V. W. Brar, G. Dresselhaus, M. S. Dresselhaus, A. K. Swan, M. S. Unlu, B. B. Goldberg, and R. Saito, Phys. Rev. B **66**, 115411 (2002).
[19] A. Jorio, A. G. Souza, G. Dresselhaus, M. S. Dresselhaus, A. K. Swan, M. S. Unlu, B. B. Goldberg, M. A. Pimenta, J. H. Hafner, C. M. Lieber, and R. Saito, Phys. Rev. B **65**, 155412 (2002).
[20] M. S. Dresselhaus, G. Dresselhaus, A. Jorio, A. G. Souza, M. A. Pimenta, and R. Saito, Acc. Chem. Res. **35**, 1070 (2002).
[21] M. S. Dresselhaus, G. Dresselhaus, A. Jorio, A. G. Souza, and R. Saito, Carbon **40**, 2043 (2002).
[22] H. Kuzmany, W. Plank, M. Hulman, Ch. Kramberger, A. Gruneis, Th. Pichler, H. Peterlik, H. Kataura, and Y. Achiba, Eur. Phys. J. B **22**, 207 (2001).
[23] A. Kukovecz, Ch. Kramberger, V. Georgakilas, M. Prato, and H. Kuzmany, Eur. Phys. J. B **28**, 223 (2002).
[24] G. Chen, G. U. Sumanasekera, B. K. Pradhan, R. Gupta, R. C. Eklund, M. J. Bronikowski, and R. E. Smalley, J. Nanosci. Nanotechnol. **2**, 621 (2002).
[25] S. Bandow, S. Asaka, Y. Saito, A. M. Rao, L. Grigorian, E. Richter, and P. C. Eklund, Phys. Rev. Lett. **80**, 3779 (1998).
[26] M. S. Strano, V. C. Moore, M. K. Miller, M. J. Allen, E. H. Haroz, C. Kittrell, R. H. Hauge, and R. E. Smalley, J. Nanosci. Nanotechnol. **3**, 81 (2003).
[27] M. S. Strano, C. A. Dyke, M. L. Usrey, P. W. Barone, M. J. Allen, H. Shan, C. Kittrell, R. H. Hauge, J. M. Tour, and R. E. Smalley, Science **301**, 1519 (2003).
[28] S. K. Doorn, R. E. Fields, H. Hu, M. A. Hamon, R. C. Haddon, J. P. Selegue, and V. Majidi, J. Am. Chem. Soc. **124**, 3169 (2002).
[29] S. K. Doorn, M. S. Strano, M. J. O'Connell, E. H. Haroz, K. L. Rialon, R. H. Hauge, and R. E. Smalley, J. Phys. Chem. B **107**, 6063 (2003).
[30] R. Krupke, F. Hennrich, H.-v. Lohneysen, and M. M. Kappes, Science **301**, 344 (2003).
[31] M. Zheng, A. Jagota, E. D. Semke, B. A. Diner, R. S. Mclean, S. R. Lustig, R. E. Richardson, and N. G. Tassi, Nat. Mater. **2**, 338 (2003).
[32] Z. Yu and L. E. Brus, J. Phys. Chem. B **105**, 6831 (2001).
[33] M. S. Strano, S. K. Doorn, E. H. Haroz, C. Kittrell, R. H. Hauge, and R. E. Smalley, Nano Lett. **3**, 1091 (2003).
[34] S. K. Doorn, D. A. Heller, P. W. Barone, M. L. Usrey, and M. S. Strano, Appl. Phys. A: Mater. Sci. Process. **78**, 1147 (2004).
[35] L. A. Girifalco, M. Hodak, and R. S. Lee, Phys. Rev. B **62**, 13104 (2000).
[36] B. Chen, M. Gao, J. M. Zuo, S. Qu, B. Liu, and Y. Huang, Appl. Phys. Lett. **83**, 3570 (2003).
[37] M. J. O'Connell, S. M. Bachilo, C. B. Huffman, V. C. Moore, M. S. Strano, E. H. Haroz, K. L. Rialon, P. J. Boul, W. H. Noon, C. Kittrell, J. Ma, R. H. Hauge, R. B. Weisman, and R. E. Smalley, Science **297**, 593 (2002).
[38] Y. K. Kwon, S. Saito, and D. Tomanek, Phys. Rev. B **58**, R13314 (1998).
[39] P. Delaney, H. J. Choi, J. Ihm, S. G. Louie, and M. L. Cohen, Nature (London) **391**, 466 (1998).
[40] P. Delaney, H. J. Choi, J. Ihm, S. G. Louie, and M. L. Cohen, Phys. Rev. B **60**, 7899 (1999).
[41] A. A. Maarouf, C. L. Kane, and E. J. Mele, Phys. Rev. B **61**, 11156 (2000).
[42] S. Reich, C. Thomsen, and P. Ordejon, Phys. Rev. B **65**, 155411 (2002).
[43] R. Saito, G. Dresselhaus, and M. S. Dresselhaus, Phys. Rev. B **61**, 2981 (2000).
[44] S. Reich and C. Thomsen, Phys. Rev. B **62**, 4273 (2000).
[45] A. G. Souza, A. Jorio, G. G. Samsonidze, G. Dresselhaus, M. S. Dresselhaus, A. K. Swan, M. S. Unlu, B. B. Goldberg, R. Saito, J. H. Hafner, C. M. Lieber, and M. A. Pimenta, Chem. Phys. Lett. **62**, 354 (2002).
[46] T. W. Odom, J. L. Huang, P. Kim, and C. M. Lieber, J. Phys. Chem. B **104**, 2794 (2000).
[47] A. Jorio, R. Saito, J. H. Hafner, C. M. Lieber, M. Hunter, T. McClure, G. Dresselhaus, and M. S. Dresselhaus, Phys. Rev. Lett. **86**, 1118 (2001).
[48] D. Kahn and J. P. Lu, Phys. Rev. B **60**, 6535 (1999).
[49] L. Henrard, E. Hernandez, P. Bernier, and A. Rubio, Phys. Rev. B **60**, R8521 (1999).
[50] L. Henrard, V. N. Popov, and A. Rubio, Phys. Rev. B **64**, 205403 (2001).
[51] V. N. Popov and L. Henrard, Phys. Rev. B **63**, 233407 (2001).
[52] M. Milnera, J. Kurti, M. Hulman, and H. Kuzmany, Phys. Rev. Lett. **84**, 1324 (2000).
[53] J. L. Sauvajol, E. Anglaret, S. Rols, and L. Alvarez, Carbon **40**, 1697 (2002).
[54] U. D. Venkateswaran, A. M. Rao, E. Richter, M. Menon, A. Rinzler, R. E. Smalley, and P. C. Eklund, Phys. Rev. B **59**, 10928 (1999).
[55] S. Lefrant, Curr. Appl. Phys. **2**, 479 (2002).
[56] A. M. Rao, J. Chen, E. Richter, U. Schlecht, P. C. Eklund, R. C. Haddon, U. D. Venkateswaran, Y. K. Kwon, and D. Tomanek, Phys. Rev. Lett. **86**, 3895 (2001).
[57] R. B. Weisman and S. M. Bachilo, Nano Lett. **3**, 1235 (2003).

[58] S. Lebedkin, F. Hennrich, T. Skipa, and M. M. Kappes, J. Phys. Chem. B **107**, 1949 (2003).
[59] J. Kurti, V. Zolyomi, M. Kertesz, and G. Sun, New J. Phys. **5**, 125 (2003).
[60] A. Gruneis, R. Saito, G. G. Somsonodze, T. Kimura, M. A. Pimenta, A. Jorio, A. G. Souza Filho, G. Dresselhaus, and M . S. Dresselhaus, Phys. Rev. B **67**, 165402 (2003).
[61] A. Thess, R. Lee, P. Nikolaev, H. Dai, P. Petit, J. Robert, C. Xu, Y. H. Lee, S. G. Kim, A. G. Rinzler, D. T. Colbert, G. E. Scuseria, D. Tomanek, J. E. Fischer, and R. E. Smalley, Science **273**, 483 (1996).
[62] A. G. Rinzler, J. Liu, H. Dai, P. Nikolaec, C. B. Huffman, F. J. Rodriguez-Macias, P. J. Boul, A. H. Lu, D. Heymann, D. T. Colbert, R. S. Lee, J. E. Fischer, A. M. Rao, P. C. Eklund, and R. E. Smalley, Appl. Phys. A: Mater. Sci. Process. **67**, 29 (1998).
[63] V. C. Moore, M. S. Strano, E. H. Haroz, R. H. Hauge, and R. E. Smalley, Nano Lett. **3**, 1379 (2003).
[64] D. Chattopadhyay, I. Galeska, and F. Papadimitrakopoulos, J. Am. Chem. Soc. **125**, 3370 (2003).